

Weakly supervised multiple instance learning histopathological tumor segmentation

Marvin Lerousseau^{1,2}, Maria Vakalopoulou^{1,2}, Marion Classe^{1,3}, Julien Adam³, Enzo Battistella^{1,2}, Alexandre Carré¹, Théo Estienne^{1,2}, Théophraste Henry¹, Eric Deutsch¹, and Nikos Paragios⁴

¹ Paris-Saclay University, Gustave Roussy, Inserm, 94800, Villejuif, France

² Paris-Saclay University, CentraleSupélec, 91190, Gif-sur-Yvette, France

³ Gustave Roussy, Pathology Department, 94800, Villejuif, France

⁴ TheraPanacea, 75014, Paris, France

Abstract. Histopathological image segmentation is a challenging and important topic in medical imaging with tremendous potential impact in clinical practice. State of the art methods relying on hand-crafted annotations that reduce the scope of the solutions since digital histology suffers from standardization and samples differ significantly between cancer phenotypes. To this end, in this paper, we propose a weakly supervised framework relying on weak standard clinical practice annotations, available in most medical centers. In particular, we exploit a multiple instance learning scheme providing a label for each instance, establishing a detailed segmentation of whole slide images. The potential of the framework is assessed with multi-centric data experiments using The Cancer Genome Atlas repository and the publicly available PatchCameleon dataset. Promising results when compared with experts' annotations demonstrate the potentials of our approach. The complete framework, including data pre-processing from TCGA download files, is available at https://github.com/marvinler/tcga_segmentation.

Keywords: weakly supervised learning · histopathological segmentation · multiple instance learning · WSI tumor segmentation

1 Introduction

In digital pathology whole slide images (WSI) are considered the golden standard for primary diagnosis [17,14]. The use of computer-assisted image analysis tools is becoming a main stream for automatic quantitative or semi-quantitative analysis for pathologists, including the discovery of novel predictive biomarkers [13]. However, the quality and the lack of standards of digital scanners on top of the tumor phenotype variability remain the main challenges for machine learning methods in this domain. A central objective in digital pathology is the accurate identification of cell or tissue of interest. Tumor tissue computational staining could be used for slide screening towards increasing the efficiency of pathologists. Automatically computed tumor maps could derive attention mechanisms for microscopic regions of interest [5], or be combined with automatic

detection of lymphocytes [16] to further characterize the tumor and immune micro-environment for treatment response prediction [3].

Traditionally, segmentation is tackled by leveraging pixel-wise or patch-wise ground-truth annotations [9]. This is highly problematic in digital pathology, notably due to the colossal size of WSIs with respect to the biological components, and the overall lack of digitization of specimens. The high variance of clinical samples contributes on the deficiency of generalization, as illustrated in [4] while for the CAMELYON16 challenge [2] front-runner solution reports 4 times higher classification errors on data from organs that were not included on training (out-of-distribution).

A standard multiple instance learning (MIL) scheme [8] deals with classifying an entity (bag) from its constituents (instances). The MIL paradigm is particularly suited to histopathological image analysis due to its ability on reasoning on subsets of data (patches) that is often a computational necessity in histopathology. The general approach of MIL consists in learning a model that embeds an instance into a latent space L . Then, the collection (usually of fixed size) of instance latent vectors is forwarded into a gathering-function which outputs the predicted bag probability, using different principles such as max-pooling [8], support vector machine [1], or even attention-based neural networks [12]. Recent large-scale histopathological studies provides promising solutions based on the MIL scheme [6,5,4]. Such diagnostics generally indicate whether a selected slide is non-neoplastic (normal), or the predicted subtype of apparent tumor tissue without really indicating the tumoral regions in the slide.

In such context, there are two different approaches of MIL: classifying bags (or slides), and training an instance classifier (or segmentation) model. For instance, studies such as [6,4,5] use max-pooling MIL and its relaxed formulation [19] to first train a segmentation-like model, and investigate various ways to combine these heatmaps predictions into a slide prediction. These works have demonstrated that MIL is viable for classifying WSI, with reported AUC for tumor vs normal slide classification above 0.99, but lack extensive evaluation for the MIL-driven segmentation performance. Noteworthily, accurate slide-based classification measures could lead to erroneous assessment regarding instance-level (i.e. segmentation) performance, as demonstrated in [11] where max-pooling based MIL is shown to recall only very discriminative tumor patches, with very high slide-level performance but very poor pixel-level qualitative performance.

In this paper, we demonstrate a weakly supervised segmentation scheme that is able to generate tumor segmentation models using annotations from conventional clinical practice of physician's assessment. The contributions of this paper are: (i) a generic meta-algorithm, generating labels from WSI binary values intended to train detailed WSI segmentation models, (ii) a training scheme providing instance-level predictions, trained only with binary WSI annotations (iii) the release of 6481 automatically generated tumor maps for publicly available slides of TCGA, an order of magnitude above previous released WSI tumor maps, (iv) an open-source solution of the formulated framework, including WSI pre-processing tools.

2 Weakly supervised learning for tissue-type segmentation in histopathological images

Contextually, we consider a set $S = \{S_i \mid 1 \leq i \leq N\}$ of N training WSIs, where each slide S_i together with their labels $T = 0, 1$ where with 0 we denote the nectitic tissue and 1 the tumor tissue. Labels T consist of binary labels indicating whether tumor tissue is present within S_i . The goal is to learn a tumor segmentation model, or a patch-based classifier, relying only on those binary annotations. In a fully supervised setup, a batch of patches $p = \{p_s \mid 1 \leq s \leq n\}$ are randomly extracted along with their annotations (binary values or microscopic segmentation maps) from each S_i in order to train a segmentation model. However, such annotations are difficult to obtain when N is quite big something really common in histopathology, so the aim of the framework is to generate a set of proxy patch-level ground truth labels by exploiting properties from the available global S_i labels.

By construction, a WSI with label 0 indicates that all extracted patches are of class 0, which is an information equivalent to a fully supervised learning scheme. However, in slides with label 1, tumor tissue could possibly be in any extent on the S_i . Alternatively, in WSI of label 1, normal tissue can theoretically cover no pixel up to the entire region in the slide except one pixel. We integrate this property by proposing a training scheme on which two parameters α and β are used in a deterministic process for each training slide of label 1:

- assign a positive label to the patches ensuring at least $\alpha\%$ are of class 1
- assign a negative label to the patches with minimum $\beta\%$ are of class 0
- discard other patches from the loss computation

In such a setup, $\alpha\%$ represents the minimum assumed relative area of tumor tissue, and similarly with $\beta\%$ the normal tissue extent. Because the explicit process is deterministic, the framework is identified by the values of α and β . It is also noteworthy that $(\alpha\%, \beta\%)$ such that $(\alpha + \beta)\% > 100$ would produce contradictory proxy labels for $100 - (\alpha + \beta)\% > 0$ for the patches, which could only impede training by diminishing the signal-to-noise ratio. Therefore, the possible space of these two parameters is defined as $\mathbb{F} = \{(\alpha, \beta); \alpha > 0, \beta \geq 0, \alpha + \beta \leq 1\}$.

Formally, given a loss function L (e.g. average binary cross-entropy or any gradient-based loss), the formulated framework aims at minimizing the following empirical risk on a training set S :

$$c_0 \cdot \sum_{\substack{S_i \in N; \\ T_{S_i} = 0}} \underbrace{\left[\sum_{p_s \sim S_i} L(f(p_s), 0) \right]}_{R_{\text{FP}}}$$

$$+ c_1 \cdot \sum_{\substack{S_i \in N; \\ T_{S_i} = 1}} \left[\underbrace{\sum_{\substack{p_s \sim S_i; \\ p_s \in P(f(p_s); \alpha, 100)}} L(f(p_s), 1)}_{R_\alpha} + \underbrace{\sum_{\substack{p_s \sim S_i; \\ p_s \in P(f(p_s); 0, \beta)}} L(f(p_s), 0)}_{R_\beta} \right]$$

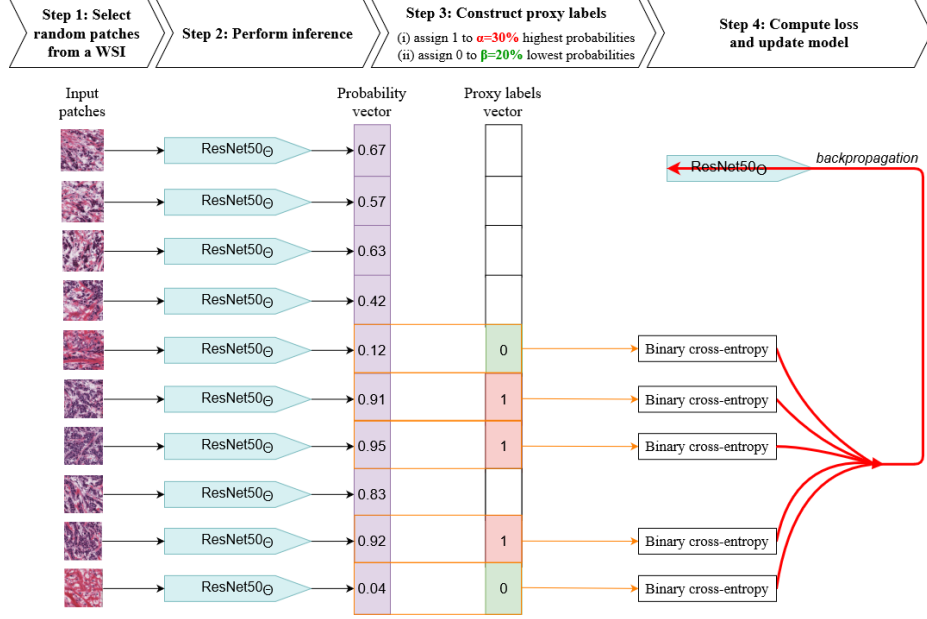


Fig. 1. Illustration of the processing of a batch of 10 patches from a positive WSI. A unique ResNet50 model with parameters θ is inferred on all images of the batch. For a given configuration of (α, β) (here, $(0.3, 0.2)$), these predictions are first used to create a proxy image-wise labels vector, then combined with the proxy label to compute batch error for further parameters θ update with backpropagation.

where $P(f(p_s); p_{\min}, p_{\max})$ is defined as the set of patches extracted from a slide S_i for which the predicted probability lies within the $p_{\min}th$ and the $p_{\max}th$ percentiles of the predictions $f(p_s)$, c_0 and c_1 are constants for batch averaging and class imbalance for both classes, and T_{S_i} refers to the binary ground-truth of WSI. Minimizing this empirical risk will guide models into recalling sufficiently enough positive or tumoral patches (R_α) per slide but not too much (R_β) while maintaining a low level of false positive in negative slides R_{FP} . The formulated approach is generic, in the sense that it can be used to train a large scope of machine learning models, including neural networks, with patch-based or pixel-wise predictions, and it can be coupled with any suited loss function. It produces trained segmentation models, readily available to produce heatmaps without intervention of the formulated pipeline nor $\alpha\%$ and $\beta\%$ parameters.

3 Implementation details and Dataset

3.1 Framework setup and Architecture details

We perform a benchmark of a representative population of the framework parameters space \mathbb{F} . Specifically, \mathbb{F} is sampled starting from 0 with increment of 0.2 (or

20%) for both α and β , resulting in $\frac{6 \cdot 7}{2} = 21$ configurations (e.g. (0, 0), (0, 0.2), (0, 0.4) and so on). Of those, the 6 configurations with $\alpha = 0$ are discarded, as this would imply that the framework provides only 0 labels contradicting with the $T_{S_i} = 1$ assumption of our empirical risk formulation. At the end only 15 sampled configurations had been used.

Each configuration is used to train a ResNet50 architecture [10], which has been shown suited for histopathology image analysis in a multitude of tasks [15], and can be used without the global average pooling layer to yield 13×13 outputs per 224 pixel-wide input image. Pre-training is used with initialization on a well-performing snapshot on ImageNet [7]. At each epoch, each training slide is sampled once. Upon sampling, a batch size of 150 patches of size 224×224 are randomly sampled at 20x magnification in the tissue region of a WSI. Data augmentation is used independently on each image, with random rotations and flips, RGB-normalization from channel-wise training averages and variances, and color jitter were also applied. The model is then concurrently inferred on the 150 patches, and a proxy-vector is constructed with the formulated pipeline as illustrated for 10 patches in Figure 1. Specifically, the $150 \times \alpha$ patches of highest probabilities are associated with a proxy value of 1, and the $150 \times \beta$ patches of lowest probabilities with a proxy value of 0. A masking vector of size 150 is concurrently filled such that patches with no attributed label are discarded. The proxy vector is then coupled with the model’s 150 predictions minus the discarded ones, to compute image-wise binary cross-entropy loss which is averaged and retro-propagated across all non masked predictions. The error signal is used to tune model parameters using Adam optimizer with learning rate of 10^{-4} and default parameters. Each configuration is trained for 20 epochs on 2 V100 NVIDIA GPU, for a training time of ~ 16 hours, or a total benchmark training time of ~ 240 hours. Finally, for our experiments we set up both c_0 and c_1 to 1 after grid search.

3.2 Dataset

The dataset consists of 6481 whole slide images from The Cancer Genome Atlas, issued from kidney (2334), bronchus and lung (2168), and breast (1979) WSIs locations. These locations were selected on TCGA as the first 3 indexed, and we perform no slide filtering nor slide selection to be coherent with standard clinical practices. This dataset was divided in training, validation and testing sets on a case basis, with 65%, 15%, and 20% of cases respectively. For the rest of the paper this test set is denoted as "In-distribution". Each selected configuration are trained using the training set, with hyper-parameters optimized on the validation set. Then, their performance is assessed on the testing set. For extensive quantitative performance assessment, expert pathologists annotated 130 slides from this testing set (45 breast, 40 kidney, 45 bronchus and lung), thus measuring in-distribution generalization. Annotations were computed at 20x magnification by a junior pathologist on a in-house annotation tool by contouring tumor tissue regions, and were modified until validation by a senior pathologist.

The same protocol was applied on additional slides extracted from locations which are not used in the previous cohort. Specifically, 35 WSIs from colon, 35 from ovary and 30 from corpus uteri are pixel-wise annotated and used to measure generalization performance of models to unseen tissue environments, which we denote as "out-of-location". We pinpoint that these annotations were not used during training nor validation, but only to assess testing segmentation performance of the produced models. For training, we use diagnostic labels extracted directly from TCGA, for which each slide name contain a code indicating the type of specimen (e.g. "Solid Tissue Normal" or "Primary Solid Tumor")⁵. Notably, normal slides are explicitly discerned from slide with apparent pathological tissue. In such context, each slide is associated with a binary value indicating whether tumor tissue is apparent in the slide, or whether the slide is of normal tissue only. To further compare with results from the community, we infer all models on the PatchCamelyon dataset [18]. The dataset consists in patches extracted from formalin-fixed, paraffin-embedded (FFPE) tissues from sentinel lympho nodes. This testing set is particularly challenging for the benchmarked models, since they are not trained on FFPE slides, which are visually highly different from flash-frozen ones.

4 Results and discussion

For performance assessment, all 15 trained ResNet50 models are inferred on the testing slides. The resulting heatmaps are compared to segmentations maps provided by the pathologists. All configurations are found to converge to super-random in-distribution performance, except for the two extrema configurations ($\alpha = 1, \beta = 0$) and (0.2, 0.8), as displayed in Table 1. The average in-distribution AUC is 0.675 ± 0.132 , with optimal AUC of 0.804 for ($\alpha = 0.2, \beta = 0.2$). Precision and recall are extracted after threshold selection on validation set and displayed in Figure 2. The α parameter seems to influence the recall at the expense of precision. Upon performance introspection by location, all configurations report the worse performance for bronchus and lung locations, with two times lower AUC performance compared to kidney and breast locations. Concerning the out-of-distribution cohort, the average AUC is 0.679 ± 0.154 , which is close to in-distribution performance, although lower when omitting bronchus and lung locations. There is no evident pattern for configurations that yield improved out-of-location results.

Some visual representations of two different samples testing are presented on Figure 3. In particular, in the figure we present the WSI image together with the pixel-wise annotations of the pathologist. Moreover, different segmentation maps depending on the configuration are also presented. One can observe that visually there are 3 or 4 configurations that are close to the expert's annotation. These configurations are in line with our quantitative results. Additional post-processing strategies would potentially boost the performance of our framework.

⁵ <https://gdc.cancer.gov/resources-tcga-users/tcga-code-tables/sample-type-codes>

Table 1. Pixelwise AUC for the 15 (α, β) framework configurations on hold-out testing set (In-distribution) and unseen testing set from locations not used in training (Out-of-location). Grey results take background into account, black ones are computed by completely discarding background.

		$\alpha = 0.2$					$\alpha = 0.4$					$\alpha = 0.6$					$\alpha = 0.8$					$\alpha = 1.0$					
		$\beta = 0$	$\beta = 0.2$	$\beta = 0.4$	$\beta = 0.6$	$\beta = 0.8$	$\beta = 1.0$	$\beta = 0$	$\beta = 0.2$	$\beta = 0.4$	$\beta = 0.6$	$\beta = 1.0$	$\beta = 0$	$\beta = 0.2$	$\beta = 0.4$	$\beta = 1.0$	$\beta = 0$	$\beta = 0.2$	$\beta = 0.4$	$\beta = 1.0$	$\beta = 0$	$\beta = 0.2$	$\beta = 0.4$	$\beta = 1.0$			
In-distribution		.786	.804	.749	.681	.566		.720	.726	.767	.685		.766	.758	.650		.589	.619		.256							
		.964	.952	.960	.930	.874		.967	.953	.959	.935		.957	.960	.940		.946	.946		.926							
Out-of-location		.866	.732	.709	.583	.257		.783	.710	.762	.658		.790	.787	.673		.785	.695		.404							
		.984	.974	.972	.958	.917		.980	.972	.978	.966		.981	.980	.968		.980	.970		.933							

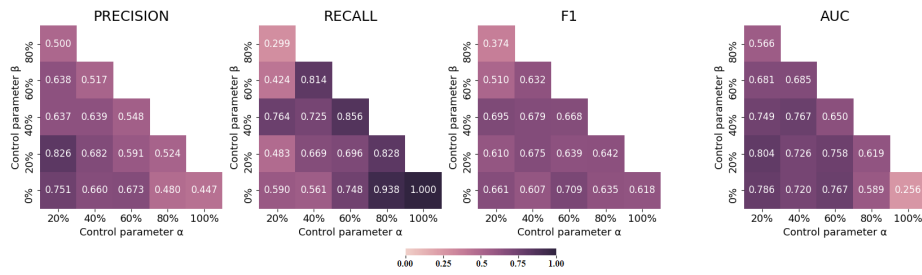


Fig. 2. Quantitative results for the 15 benchmarked configurations on the hold-out testing set from bronchus and lung, kidney, and breast locations. Each subplot (4 in total) displays a pixelwise measure, as indicated in its sup-title, for each configuration in a matrix format. AUC: area under the ROC curve.

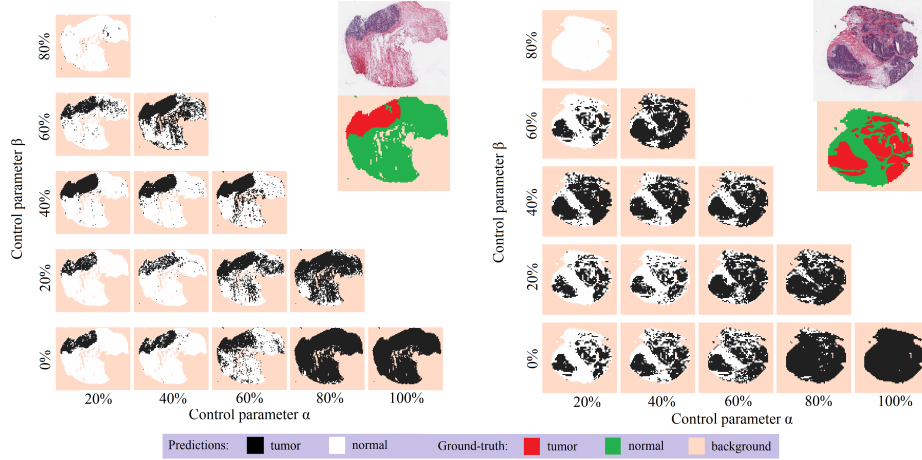


Fig. 3. Unfiltered predicted tumor maps on hold-out testing samples for the 15 benchmarked framework configurations. 2 WSI and their corresponding results are displayed in a matrix-format.

To test the generalization of our method, we performed also experiments on the PatchCamelyon dataset [18]. In particular we found the most of the configurations (12 out of the 15) reporting quite low AUC, between 0.428 and 0.612. However, 3 configurations are found to generalize to some extent, that is ($\alpha = 0.2, \beta = 0$) with 0.672 AUC, (0.2, 0.2) with 0.802, and (0.4, 0) with 0.758. Although these results are far from report AUC of 0.963 obtained with fully supervised models specifically trained on this dataset [18], the results suggest the presented framework could train models which can grasp generic discriminative cancer features from multiple types of slides in broad biological context.

5 Conclusion and future works

In this paper we propose a weakly supervised model with provides segmentation maps of WSIs, trained only with binary annotations over the entire WSIs. From our experiments we saw that usually 3 to 4 configurations are expected to yield respectively high precision, high recall, and high overall performance for WSIs of different organs and tumor coverage. The findings in this paper highlight the potential of weakly supervised learning in histopathological image analysis, which is known to be heavily impeded by annotation bottleneck. With the complete open-source releases of both the complete WSI pre-processing pipeline, the presented training framework, as well as the inference pipeline, the presented approach can be used off-the-shelf for pan-cancer tumor segmentation using its entire 18k flash-frozen WSI, or other type of tissue segmentation, such as necrosis or stromal tissue. The public release of 6481 automatically generated tumor maps, with an expected AUC above 0.932, should lower the barrier of entry to pathomics by bypassing tumor annotation efforts. All code and results can be found at https://github.com/marvinler/tcga_segmentation.

There are many ways to fine-tune a segmentation model using the formulated framework, such as with more appropriate deep learning architectures or with more extensive hyper-parameters optimization. We believe the most impactful future works will revolve around the proxy-generation labels from more sophisticated slide labels which would yield higher information while remaining fast to obtain, essentially trading annotation time for performance.

References

1. Andrews, S., Tschantaridis, I., Hofmann, T.: Support vector machines for multiple-instance learning. In: Advances in neural information processing systems. pp. 577–584 (2003)
2. Bejnordi, B.E., Veta, M., Van Diest, P.J., Van Ginneken, B., Karssemeijer, N., Litjens, G., Van Der Laak, J.A., Hermans, M., Manson, Q.F., Balkenhol, M., et al.: Diagnostic assessment of deep learning algorithms for detection of lymph node metastases in women with breast cancer. *Jama* **318**(22), 2199–2210 (2017)
3. Binnewies, M., Roberts, E.W., Kersten, K., Chan, V., Fearon, D.F., Merad, M., Coussens, L.M., Gabrilovich, D.I., Ostrand-Rosenberg, S., Hedrick, C.C., et al.:

Understanding the tumor immune microenvironment (time) for effective therapy. *Nature medicine* **24**(5), 541–550 (2018)

4. Campanella, G., Hanna, M.G., Geneslaw, L., Miraflor, A., Silva, V.W.K., Busam, K.J., Brogi, E., Reuter, V.E., Klimstra, D.S., Fuchs, T.J.: Clinical-grade computational pathology using weakly supervised deep learning on whole slide images. *Nature medicine* **25**(8), 1301–1309 (2019)
5. Campanella, G., Silva, V.W.K., Fuchs, T.J.: Terabyte-scale deep multiple instance learning for classification and localization in pathology. *arXiv preprint arXiv:1805.06983* (2018)
6. Coudray, N., Ocampo, P.S., Sakellaropoulos, T., Narula, N., Snuderl, M., Fenyö, D., Moreira, A.L., Razavian, N., Tsirigos, A.: Classification and mutation prediction from non-small cell lung cancer histopathology images using deep learning. *Nature medicine* **24**(10), 1559 (2018)
7. Deng, J., Dong, W., Socher, R., Li, L.J., Li, K., Fei-Fei, L.: Imagenet: A large-scale hierarchical image database. In: *2009 IEEE conference on computer vision and pattern recognition*. pp. 248–255. Ieee (2009)
8. Dietterich, T.G., Lathrop, R.H., Lozano-Pérez, T.: Solving the multiple instance problem with axis-parallel rectangles. *Artificial intelligence* **89**(1-2), 31–71 (1997)
9. Guo, Y., Liu, Y., Georgiou, T., Lew, M.S.: A review of semantic segmentation using deep neural networks. *International journal of multimedia information retrieval* **7**(2), 87–93 (2018)
10. He, K., Zhang, X., Ren, S., Sun, J.: Deep residual learning for image recognition. In: *Proceedings of the IEEE conference on computer vision and pattern recognition*. pp. 770–778 (2016)
11. Hou, L., Samaras, D., Kurc, T.M., Gao, Y., Davis, J.E., Saltz, J.H.: Patch-based convolutional neural network for whole slide tissue image classification. In: *Proceedings of the IEEE Conference on Computer Vision and Pattern Recognition*. pp. 2424–2433 (2016)
12. Ilse, M., Tomczak, J.M., Welling, M.: Attention-based deep multiple instance learning. *arXiv preprint arXiv:1802.04712* (2018)
13. Janowczyk, A., Madabhushi, A.: Deep learning for digital pathology image analysis: A comprehensive tutorial with selected use cases. *Journal of pathology informatics* **7** (2016)
14. Jara-Lazaro, A.R., Thamboo, T.P., Teh, M., Tan, P.H.: Digital pathology: exploring its applications in diagnostic surgical pathology practice. *Pathology* **42**(6), 512–518 (2010)
15. Mormont, R., Geurts, P., Marée, R.: Comparison of deep transfer learning strategies for digital pathology. In: *Proceedings of the IEEE Conference on Computer Vision and Pattern Recognition Workshops*. pp. 2262–2271 (2018)
16. Saltz, J., Gupta, R., Hou, L., Kurc, T., Singh, P., Nguyen, V., Samaras, D., Shroyer, K.R., Zhao, T., Batiste, R., et al.: Spatial organization and molecular correlation of tumor-infiltrating lymphocytes using deep learning on pathology images. *Cell reports* **23**(1), 181–193 (2018)
17. Stathonikos, N., Veta, M., Huisman, A., van Diest, P.J.: Going fully digital: Perspective of a dutch academic pathology lab. *Journal of pathology informatics* **4** (2013)
18. Veeling, B.S., Linmans, J., Winkens, J., Cohen, T., Welling, M.: Rotation equivariant cnns for digital pathology. In: *International Conference on Medical image computing and computer-assisted intervention*. pp. 210–218. Springer (2018)

19. Zhu, W., Lou, Q., Vang, Y.S., Xie, X.: Deep multi-instance networks with sparse label assignment for whole mammogram classification. In: International Conference on Medical Image Computing and Computer-Assisted Intervention. pp. 603–611. Springer (2017)